

# Classifying galaxies according to their H I content

Sambatra Andrianomena,<sup>1,2★</sup> Mika Rafieferantsoa<sup>2,3,4</sup> and Romeel Davé<sup>1b,2,3,5</sup>

<sup>1</sup>South African Radio Astronomy Observatory (SARAO), Black River Park, Observatory, Cape Town 7925, South Africa

<sup>2</sup>University of the Western Cape, Bellville, Cape Town 7535, South Africa

<sup>3</sup>South African Astronomical Observatory, Observatory, Cape Town 7925, South Africa

<sup>4</sup>Max-Planck-Institut für Astrophysik, Karl-Schwarzschild-Str. 1, 85748 Garching, Germany

<sup>5</sup>Institute for Astronomy, Royal Observatory, University of Edinburgh, Edinburgh EH9 3HJ, UK

Accepted 2020 January 20. Received 2020 January 20; in original form 2019 June 12

## ABSTRACT

We use machine learning to classify galaxies according to their H I content, based on both their optical photometry and environmental properties. The data used for our analyses are the outputs in the range  $z = 0-1$  from MUFASA cosmological hydrodynamic simulation. In our previous paper, where we predicted the galaxy H I content using the same input features, H I-rich galaxies were only selected for the training. In order for the predictions on real observation data to be more accurate, the classifiers built in this study will first establish if a galaxy is H I rich ( $\log(M_{\text{HI}}/M_*) > -2$ ) before estimating its neutral hydrogen content using the regressors developed in the first paper. We resort to various machine-learning algorithms and assess their performance with some metrics such as *accuracy*,  $f_1$ , AUC PR, *precision*, *specificity*, and *log loss*. The performance of the classifiers, as opposed to that of the regressors in previous paper, gets better with increasing redshift and reaches their peak performance around  $z = 1$  then starts to decline at even higher  $z$ . Random forest method, the most robust among the classifiers when considering only the mock data for both training and test in this study, reaches an accuracy above 98.6 per cent at  $z = 0$  and above 99.0 per cent at  $z = 1$ , which translates to an AUC PR above 99.93 per cent at low redshift and above 99.98 per cent at higher one. We test our algorithms, trained with simulation data, on classification of the galaxies in RESOLVE, ALFALFA, and GASS surveys. Interestingly, SVM algorithm, the best classifier for the tests, achieves a *precision*, the relevant metric for the tests, above 87.60 per cent and a *specificity* above 71.4 per cent with all the tests, indicating that the classifier is capable of learning from the simulated data to classify H I-rich/H I-poor galaxies from the real observation data. With the advent of large H I 21 cm surveys such as the SKA, this set of classifiers, together with the regressors developed in the first paper, will be part of a pipeline, a very useful tool, which is aimed at predicting H I content of galaxies.

**Key words:** galaxies: evolution – galaxies: statistics.

## 1 INTRODUCTION

Much effort has been put into understanding the role of neutral hydrogen in galaxy formation and evolution. In the canonical picture based on the Hubble Sequence, the spiral galaxies are rich in cold gas and star forming, whereas the ellipticals are red and quiescent. However, an increasing number of observational evidence shows that these correlations are not always true. Local early-type galaxies from the ATLAS<sup>3d</sup> survey were shown to contain significant cold gaseous components (Davis et al. 2011). They found that the relative angles between the gaseous and stellar planes show a bimodal distribution, but found no plausible explanation

for such difference. This indicates that the gas distribution of a galaxy does not necessarily follow that of the stellar component. Therefore, direct inference of the gas content of galaxy based on its optical content is inaccurate. Elliptical galaxies are observed to form stars in cool core massive clusters (Donahue et al. 2011) that is suggestive of the presence of cold gas in those objects. The amount of gas components in massive ellipticals is crucial to understanding the evolution and growth of galaxies at the massive end, but the presence of kinematic abnormalities in their gas content as well as the uncertain effects of the active galactic nuclei feedback can affect the surface density of the gas content to pull the galaxies below the H I detection limit, especially at higher redshifts.

Spiral galaxies are gas rich, but the limitations of observing the neutral gas at intermediate redshift prevent a robust study of the evolution of their gas content. Low-redshift ( $z \lesssim 0.4$ ) H I can

\* E-mail: andrianomena@gmail.com

be observed with the 21cm emission line to provide the neutral hydrogen mass distribution of nearby galaxies. For instance, the Arecibo Legacy Fast ALFA (ALFALFA; Haynes et al. 2018) observed  $\sim 30\,000$  galaxy H I fluxes. The highest redshift galaxy ( $z = 0.376$ ) detected in 21 cm emission was observed with the COSMOS H I Large Extragalactic Survey (Fernández et al. 2016). At any substantially higher redshift, the H I content of galaxies is inferred from damped Lyman alpha systems (DLAs) in the spectra of background quasars, but it is difficult to measure the H I mass from DLAs, and the relationship between galaxies and DLAs is not completely clear. The upcoming blind surveys such as Looking At the Distant Universe with the MeerKAT Array (LADUMA) on MeerKAT and eventually follow-up surveys on the SKA (Square Kilometre Array) aim to measure the H I content of galaxies at intermediate redshifts, to  $z \sim 1$  and beyond.

The gas content of satellite galaxies are substantially impacted by environmental effects. Observationally, only 25 per cent of  $\alpha.40$  (ALFALFA 40 per cent; Haynes et al. 2011) galaxies were found to be in groups or clusters (Hess & Wilcots 2013), which is lower than for the overall galaxy population. They found that in contrast to increasing optical sources towards to the centre of groups or clusters, the number of H I sources decreases. This is also supported from theoretical views. Using hydrodynamical simulation, Rafieferantsoa et al. (2015) showed that the fraction of H I deficient galaxies increases towards higher halo masses. This is related to the star formation quenching time-scale decrease towards higher halo mass: from  $>3$  Gyr for  $M_{\text{halo}} < 10^{12} M_{\odot}$  to  $<1$  Gyr for  $M_{\text{halo}} > 10^{13} M_{\odot}$  (Rafieferantsoa, Davé & Naab 2019). Recent observational work by Foltz et al. (2018) agrees with this prediction, but in contrast Fossati et al. (2017) argue for no relationship between galaxy quenching time-scales and halo mass. Simulations also suggest that the presence of H I is strongly correlated with star formation, even if the star formation is physically occurring in molecular gas (Davé et al. 2017). Therefore, the H I content appears to have a complex relationship with respect to stellar mass, star formation rate, morphology, and environment. This makes it challenging to predict what the H I content of any given galaxy will be without accounting for the full range of its properties.

In order to better design and interpret upcoming H I surveys, it is useful to be able to estimate the expected H I content of galaxies that will be observed based on their already-measured multiwavelength properties. To do so, here we develop and employ galaxy classification tools using machine learning. Galaxy classification is a very useful approach as it can provide insights into the physical processes by which galaxies evolve over cosmic time. There exist different and complementary ways to classify galaxies depending on the availability of the data, for instance morphological classification or spectral classification. The Hubble Sequence focuses on morphological classification, while spectral classification via absorption and emission lines provides more information about the chemical composition and stellar populations of galaxies (Morgan & Mayall 1957). Zaritsky, Zabludoff & Willick (1995) developed a  $\chi^2$ -fitting approach to identify the best linear combination of template spectra that matches the observed spectrum in order to classify galaxies spectroscopically with low signal-to-noise ratio (S/N), and found good correlations of  $\geq 80$  per cent between spectra and morphology from *Hubble* classification. Slonim et al. (2001) presented a novel *information bottleneck* (IB) approach, improving on the then-standard geometrical and statistical approaches, to classify galaxy spectra using 2dF Galaxy Survey (Colless, Morganti & Couch 1998; Folkes et al. 1999). In a seminal work, Fukugita et al. (2007) conducted morphological classification

of galaxies which was achieved by simple visual inspection where volunteers catalogued thousands of objects from Sloan Digital Sky Survey Data Release 3 (SDSS DR3; York et al. 2000) in order to obtain the rate of interacting galaxies. The need for automated classification arose with the increasing amount of available survey data, and it was demonstrated by Naim et al. (1995) and Lahav et al. (1996) that accuracy achieved by a trained *artificial neural network* in classifying galaxies is comparable to that of a human expert. In a morphological classification of high-redshift galaxies that Huertas-Company et al. (2008) conducted using *SVMs*, they argued that at  $z > 1$  early-type galaxies were underestimated in the classifications using sample from COSMOS *Hubble Space Telescope (HST)/Advanced Camera for Surveys (ACS)* (Koekemoer et al. 2007) owing to the effects of morphological *k*-correction. In galaxy morphological classification, tree-based algorithms have also proved to be relatively robust classifier compared to other machine-learning algorithms, as reported by Gauci, Adami & Abela (2010). Hence, there is a long history of using sophisticated galaxy classification methods in astronomy, but so far this has not been extensively applied to studying H I.

In our previous work in Rafieferantsoa, Andrianomena & Davé (2018) (RAD18 hereafter), we investigated the possibility of estimating the H I content of galaxies using a variety of machine-learning algorithms. Considering both the optical and environmental properties of the galaxies as input features, the algorithms were trained using large subsets of data from MUFASA simulation and tested on different subsets. They found that the performance of all regressors – assessed by using root mean squared error (RMSE) and Pearson’s correlation coefficient ( $\mathbf{r}$ ) as metrics – degraded at higher redshift. Despite the tendency of all learners to underpredict the high H I richness and overpredict the low one, random forest (RF) method – followed tightly by deep neural network (DNN) – exhibited an overall best performance; achieving an RMSE  $\sim 0.25$  (corresponding to  $\mathbf{r} \sim 0.9$ ) at  $z = 0$ . They then applied the regressors to real data from two different surveys, RESolved Spectroscopy Of Local VolumE (RESOLVE Stark et al. 2016) and ALFALFA. To this end, they trained the algorithms with an output from MUFASA at  $z = 0$  and used them to predict the H I content of galaxies from real observations. Their results proved that the learners which they built can be potentially used for H I study with the upcoming large H I surveys like the SKA. Prior to this work, related study by Teimoorinia, Ellison & Patton (2017) also investigated the estimation of H I content of galaxies based on the SDSS and ALFALFA data using 15 derived galaxy parameters.

However, in RAD18 we only considered H I-rich galaxies ( $\log(M_{\text{H I}}/M_{*}) \geq -2$ ), hence the machine-learning methods were trained to predict the gas content of H I-rich galaxies only. Therefore, at this stage, those algorithms on their own cannot be deployed in real world application where not all galaxies will be H I rich. Models generally predict that galaxies are bimodal in their H I content, particularly since satellite galaxies lose their H I quite rapidly, after a delay period, once they enter another halo (Rafieferantsoa et al. 2019). To extend our work to be more generally applicable, we therefore need a way to classify galaxies as H I-rich or H I-poor based on available photometric data.

In this follow-up paper, we address this issue by building a set of learners that filter out the H I-poor galaxies in real survey, such that the regressors built in RAD18 only predict galaxy gas content known to be above a certain threshold. Together with the classifiers, the regressors will form a pipeline which will be used to estimate H I gas of galaxies in real observation. The approach is to use the same set of input features as in RAD18 for the classification. This

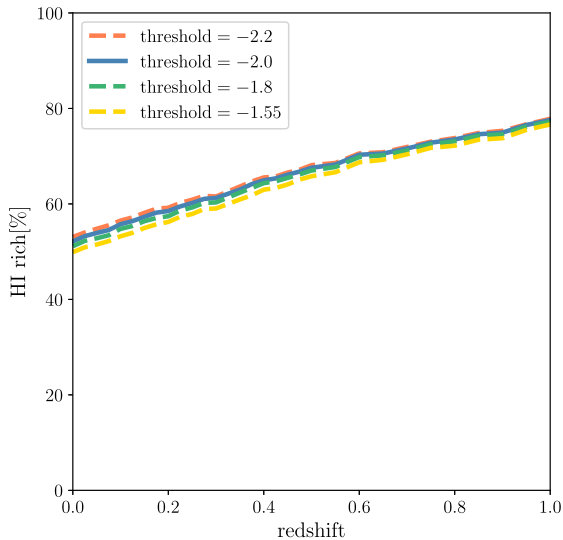


**Figure 1.** Percentage of HI-rich galaxies in our sample as a function of redshift bin for four different values of HI-richness threshold considered. In total, including all bins up to  $z = 1$ , there are about 64 per cent positive sample when considering a threshold = -2.

paper thus extends our approach to be more generally applicable to any galaxy survey that contains the requisite input features, which are chosen to be typically observationally accessible in present and upcoming multiwavelength surveys.

We present our machine-learning setup for our analyses in Section 2 and list all the algorithms we consider in Section 3. The results are shown in Section 4 and we demonstrate how the methods can be applied to data from real surveys in Section 5. We finally conclude in Section 6.

## 2 SETUPS

It is first noted that we make use of the same outputs ( $z = 0-1$ ) from MUFASA simulation to build our classifiers. Considering the Planck cosmological parameters  $\Omega_m = 0.3$ ,  $\Omega_\Lambda = 0.7$ ,  $\Omega_b = 0.048$ ,  $H_0 = 68 \text{ km s}^{-1} \text{ Mpc}^{-1}$ ,  $\sigma_8 = 0.82$ , and  $n_s = 0.97$  (Planck et al. 2016), each snapshot results from simulating a comoving box of  $50h^{-1} \text{ Mpc}$  with a resolution of  $N = 512^3$  for each species (dark matter and gas). For the training, the features  $\{u, g, r, i, z, U, V, J, H, K_s, \Sigma_3, v_{\text{gal}}\}$  are considered whereas our target – as in the case of a binary classification – is one of the two classes;  $0$  to denote HI-depleted galaxies ( $\log(M_{\text{HI}}/M_*) < v_{\text{thresh}}$ ) and  $1$  for HI-rich galaxies ( $\log(M_{\text{HI}}/M_*) \geq v_{\text{thresh}}$ ). To split the galaxies into two classes, one simply needs to run through all galaxies in the data and assign  $0$  or  $1$  to it if its gas content is below or above the threshold value  $v_{\text{thresh}}$ . In our case, we adopt  $v_{\text{thresh}} = -2$ , i.e. the HI content is 2 orders of magnitude fewer than the stellar content. In Fig. 1, we show the variation of the positive class in a sample as a function of redshift. The trend can be attributed to the higher cosmological gas accretion at higher redshift, resulting in most of them to be HI rich (Davé et al. 2017). However while evolving to present, they go through different mechanisms that can deplete/decrease their HI content, hence the number of HI-rich galaxies is expected to be relatively smaller at lower redshift.

As in RAD18, we adopt different setups both in terms of features and type of training which we present again in Table 1 for reference. For ‘ $z$ -training’, a classifier is built at each redshift bin, whereas for ‘ $f$ -training’ we make use of all data available in the range  $z = 0-0.5$ .

In contrast with the  $f$ -training in RAD18, we do not go to higher  $z$  to train the learner. In all cases 80 per cent of the data are used for training and the remaining are used for testing.

## 3 ALGORITHMS

We used a rather wide variety of machine-learning algorithms in RAD18 to see which one captures best the features from the data in order to make good predictions. Having gained a better understanding about how the methods dealt with information from the data, we consider most of them for this classification problem. It is worth reiterating that as opposed to regression task where the label is a numerical variable, the label for a classification task is a class – represented by integers mainly.<sup>1</sup>

*$k$ -nearest neighbour – classification:* the principle remains the same as in regression but instead of averaging the targets of  $k$ -closest neighbours to make prediction, the predicted class  $y_{\text{new}}$  of a new instance  $\mathbf{x}_{\text{new}}$  is simply the majority of the classes of  $k$ -neighbours of  $\mathbf{x}_{\text{new}}$ .

*Random forest and Gradient boosting – classification:* decision tree is still the base estimator of both RF and GRAD (gradient boosting). In contrast with its regressor counterpart, the decision tree classifier splits the training set at a split point  $s_i$  using a feature  $i$ . The splitting is done in such a way as to minimize the objective function

$$\mathcal{F} = \frac{n_{R_1}}{n} G_{R_1} + \frac{n_{R_2}}{n} G_{R_2}, \quad (1)$$

where  $n_{R_1}$  is the number of examples in region  $R_1$  and  $n_{R_2}$  the number of examples in  $R_2$ . The total number of instances  $n$  before the split is simply  $n = n_{R_1} + n_{R_2}$ . The Gini impurity<sup>2</sup>  $G$  of each region is given by

$$G = 1 - \sum_{i=1}^k p_i^2, \quad (2)$$

where  $p_i$  is the probability of an instance to belong to a class  $i$  in the region. This can be computed by the ratio between the number of instances belonging to a class  $i$  and the number of all instances in the region. The splitting can be done recursively on the resulting nodes depending on the required size of the tree. The RF method predicts the class of a new instance  $\mathbf{x}_{\text{new}}$  by aggregating the predictions of all its decision trees. The expression of the GRAD classifier is quite similar to equation (6) in RAD18.

*Deep neural network – classification:* in contrast with the DNN regressor, the activation function of the output layer is a sigmoid function<sup>3</sup>

$$\sigma(x) = \frac{1}{1 + e^{-x}}, \quad (3)$$

which computes the probability  $p_i$  that an instance belongs to class  $i$ . In this case specifically, if  $p \geq 0.5$ ,  $y_{\text{new}}$  is  $1$  (positive class) whereas for  $p < 0.5$   $y_{\text{new}}$  is  $0$  (negative class). The objective function, known as *log loss*, is defined as

$$\mathcal{F} = -\frac{1}{N} \sum_{i=1}^N y_i \log(p_i) + (1 - y_i) \log(1 - p_i). \quad (4)$$

The weights and biases are updated via backpropagation as usual. The cost function in equation (4) can be generalized for multiclass

<sup>1</sup>Categorical variable.

<sup>2</sup>Also called Gini index.

<sup>3</sup>Also named *logit*.

**Table 1.** List of all the setups that are considered in the analysis. For easy reference, each setup has been given a name.

Name	Surveys	Features	Target	Description
fSMg	SDSS	$u, g, r, i, z, v_{\text{gal}}, \Sigma_3$	$\log(M_{\text{H1}}/M_*)$	Redshift information not required
fSClr	SDSS	colour indices, $v_{\text{gal}}, \Sigma_3$	$\log(M_{\text{H1}}/M_*)$	Redshift information not required
fSCmb	SDSS	colour indices, $u, g, r, i, z, v_{\text{gal}}, \Sigma_3$	$\log(M_{\text{H1}}/M_*)$	Redshift information not required
fAMg	SDSS+Johnson + 2MASS	$H, J, K_s, U, V, u, g, r, i, z, v_{\text{gal}}, \Sigma_3$	$\log(M_{\text{H1}}/M_*)$	Redshift information not required
fAClr	SDSS+Johnson + 2MASS	colour indices, $v_{\text{gal}}, \Sigma_3$	$\log(M_{\text{H1}}/M_*)$	Redshift information not required
zSMg	SDSS	$u, g, r, i, z, v_{\text{gal}}, \Sigma_3$	$\log(M_{\text{H1}}/M_*)$	Prediction at a given redshift bin
zSClr	SDSS	colour indices, $v_{\text{gal}}, \Sigma_3$	$\log(M_{\text{H1}}/M_*)$	Prediction at a given redshift bin
zSCmb	SDSS	colour indices, $u, g, r, i, z, v_{\text{gal}}, \Sigma_3$	$\log(M_{\text{H1}}/M_*)$	Prediction at a given redshift bin
zAMg	SDSS+Johnson + 2MASS	$H, J, K_s, U, V, u, r, r, i, z, v_{\text{gal}}, \Sigma_3$	$\log(M_{\text{H1}}/M_*)$	Prediction at a given redshift bin
zAClr	SDSS+Johnson + 2MASS	colour indices, $v_{\text{gal}}, \Sigma_3$	$\log(M_{\text{H1}}/M_*)$	Prediction at a given redshift bin

case by using what is called *cross entropy* defined as

$$\mathcal{F} = -\frac{1}{N} \sum_{i=1}^N \sum_{k=1}^{\mathcal{K}} y_k^i \log(p_k^i), \quad (5)$$

where  $\mathcal{K}$  is number of classes.

#### 4 GALAXY CLASSIFICATION

The objective in this work is to be able to establish whether a galaxy is H I rich or H I poor by exploiting both its optical and environmental data. To do so, we build various classifiers (see Section 3) and compare their performance qualitatively. But first, we introduce some useful terminology in machine learning. *TP* and *TN* are *true positive* – number of instances that are correctly predicted by the classifier to belong to 1 – and *true negative* – number of instances that are correctly predicted by the classifier to belong to 0 – respectively. *FN* or *false negative* denotes the number of instances that belong to 1 but are classified as 0 and *FP* or *false positive* indicates the number of instances that belong to 0 but are predicted as 1. A confusion matrix, in such binary classification is a  $2 \times 2$  ( $n \times n$  in multiclass case) matrix that summarizes the predictions of a classifier on a test set. The quality of such matrix will be quantified by the following metrics.

*Accuracy*: in binary classification,<sup>4</sup> it measures the ratio of the correct predictions on a test sample, i.e.

$$\text{accuracy} = \frac{\text{TP} + \text{TN}}{\text{FN} + \text{FP} + \text{TP} + \text{TN}}, \quad (6)$$

*Precision*: it indicates how well the algorithm minimizes the number of instances incorrectly identified as a *positive class* (*FP*) and is given by

$$\text{precision} = \frac{\text{TP}}{\text{TP} + \text{FP}}. \quad (7)$$

A good precision (high value close to one) translates to low *FP*.

*Recall*: also called *sensitivity*, it characterizes the ability of the method to minimize the number of instances wrongly identified as a *negative class* (*FN*). It is given by

$$\text{recall} = \frac{\text{TP}}{\text{TP} + \text{FN}}. \quad (8)$$

It is worth noting that, provided a classifier, if *FP* increases then *FN* decreases and vice versa. In other words, an increase in *precision* implies a decrease in *recall* – the so called *precision-recall* trade-off. In our case, since we are mainly interested in identifying H I-rich

galaxies whose gas content is to be predicted by our regressors built in RAD18, we require our classifier to have good *precision*, as having a learner with a lower *FP* (hence higher *FN*) – lower number of H I-poor galaxies predicted to belong to class of H I-rich galaxies – is in our case more preferable than a learner with a lower *FN*, hence higher *FP*.

*F<sub>1</sub> score*: this metric which combines *precision* and *recall* is their harmonic mean, given by

$$F_1 = \frac{\text{TP}}{\text{TP} + \frac{\text{FN} + \text{FP}}{2}}. \quad (9)$$

High *F<sub>1</sub>* score simply means that both *precision* and *recall* are also high, which is the ideal case.

*Log loss*: this quantity, given by equation (4), is also used as a metric. The lower its value, the better the classifier is.

*Receiving operating characteristic – area under the curve (ROC AUC)*: it is also possible to plot *recall* against *FP* rate which is given by  $1 - \text{specificity}$  where

$$\text{specificity} = \frac{\text{TN}}{\text{TN} + \text{FP}}.$$

As can be seen from equations (7) and (8), *FP* follows the increase of *recall* as a consequence of the *precision-recall* trade-off. Another measure of the performance of a classifier is then to compute the area under the curve (*recall versus FP* rate). A perfect learner would have *ROC AUC* = 1.

*Area under the curve – precision recall (AUC-PR)*: positive predictive value (precision) *versus* true positive rate (recall) curve to assess a classifier performance in the case of imbalanced sample.

A binary classifier uses a threshold parameter such that a new instance will be classified as *positive* or *negative* if the predicted probability is above or below the threshold respectively. A *precision-recall* (alternatively *recall-FP* rate) pair corresponds to a single value of a threshold parameter of a classifier and the idea behind the *ROC* curve is to find the best pair values *precision-recall* (alternatively *recall-FP* rate) in order to mitigate the trade-off between them, i.e. finding a threshold parameter value of the classifier such that both *precision* and *recall* are high. The results are now presented in the following.

##### 4.1 Dependence on redshift

Table 1 lists the various setups that we feed to our machine-learning algorithms. The name specifies whether it uses *f*-training or *z*-training, whether we use SDSS data only (S) or all data including near-IR (A), and whether we use magnitudes (Mg) or colors (Clr) or combine them (Cmb). In all cases, we use environment as measured

<sup>4</sup>And even in multiclass case.

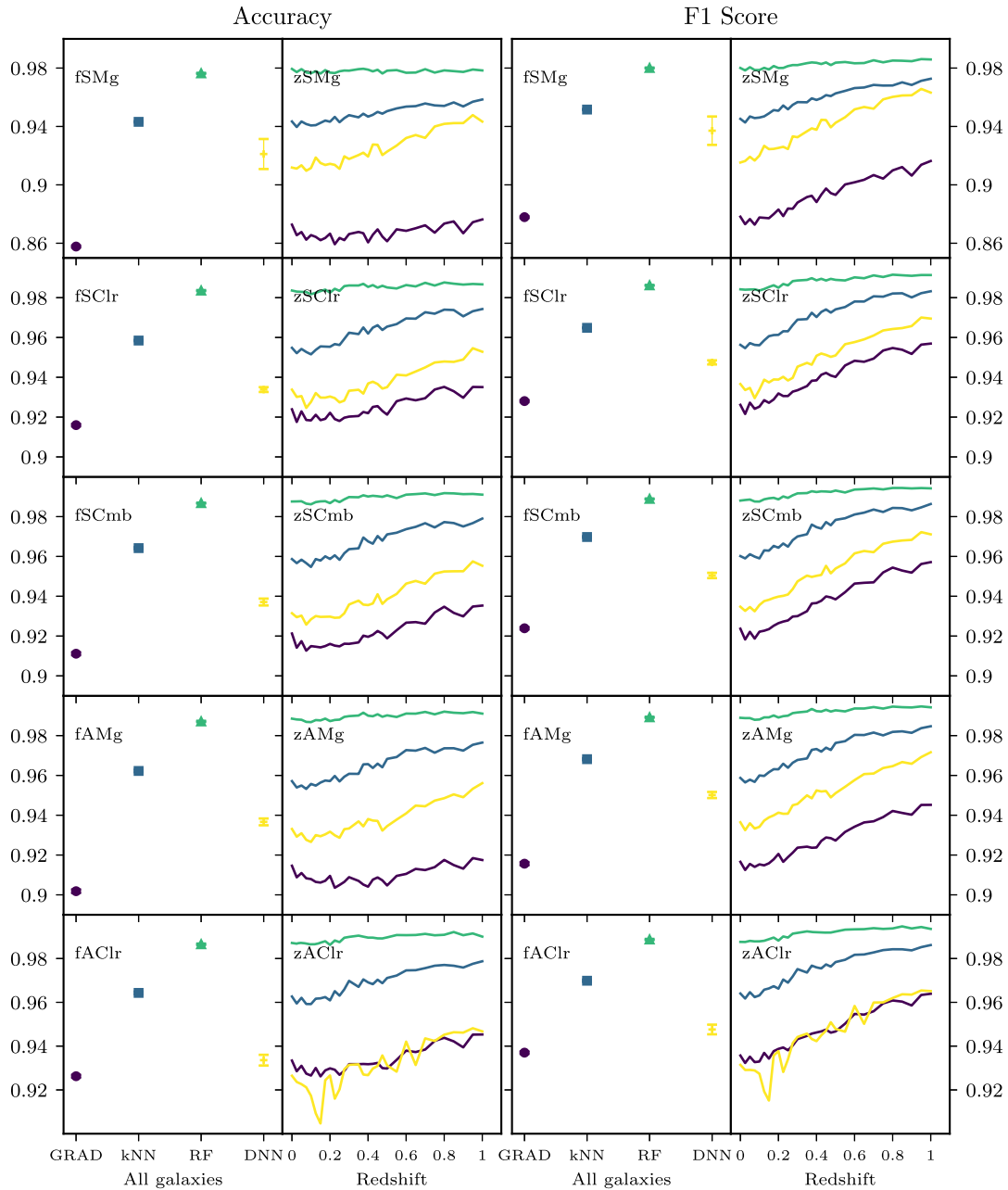


**Figure 2.** Accuracy and  $f_1$  are shown on the two columns from the left and right, respectively. Good performance means high values of both accuracy and  $f_1$ . The dots, colour coded by the training models we use, represent the performance (accuracy and  $f_1$ ) of each classifier trained on all the data available between  $z = 0-0.5$ , ‘ $f$ -training’. In the same way, the lines denote the value of the two metrics of each learner as a function of redshift ‘ $z$ -training’. Each row shows different results for different setups. The accuracy values are shown on the left y-axes and the  $f_1$  values on the right y-axes. The results presented here are obtained from using 20 percent of a sample at each bin for  $z$ -training and 20 percent of the whole data set for  $f$ -training. The error bars are obtained from running training/testing  $10\times$  by fixing a different number of the random state when splitting the data set into train and test sets.

by the third nearest neighbour ( $\Sigma_3$ ), as well as the galaxy peculiar velocity ( $v_{\text{gal}}$ ).

In Fig. 2, we show the results corresponding to each classifier selected in our investigation, considering only two metrics here, accuracy and  $f_1$ , for illustration purpose. The first column shows the accuracy achieved by each method with different input features for ‘ $f$ -training’, the second column is the resulting accuracy for ‘ $z$ -training’, the third column presents the  $f_1$  score for ‘ $f$ -training’ and finally the fourth one is the  $f_1$  score for ‘ $z$ -training’.

Most classifiers attain accuracy and  $f_1$  scores exceeding 0.9, which indicates that it is robustly possible to classify galaxies into H I rich versus H I poor based on observable properties, at least in the idealized case of training and testing on simulated data alone. Still, there are clear differences among the classifiers. RF (green) clearly exhibits the best performance whereas GRAD (purple) is relatively the weakest. For instance, RF (‘ $z$ -training’) accuracy and  $f_1$  both reach  $\sim 0.98$  at  $z = 0$  and  $\sim 0.99$  at  $z = 1$ , with similar values when combining data from  $z = 0$  to  $0.5$  (‘ $f$ -training’). kNN (k-

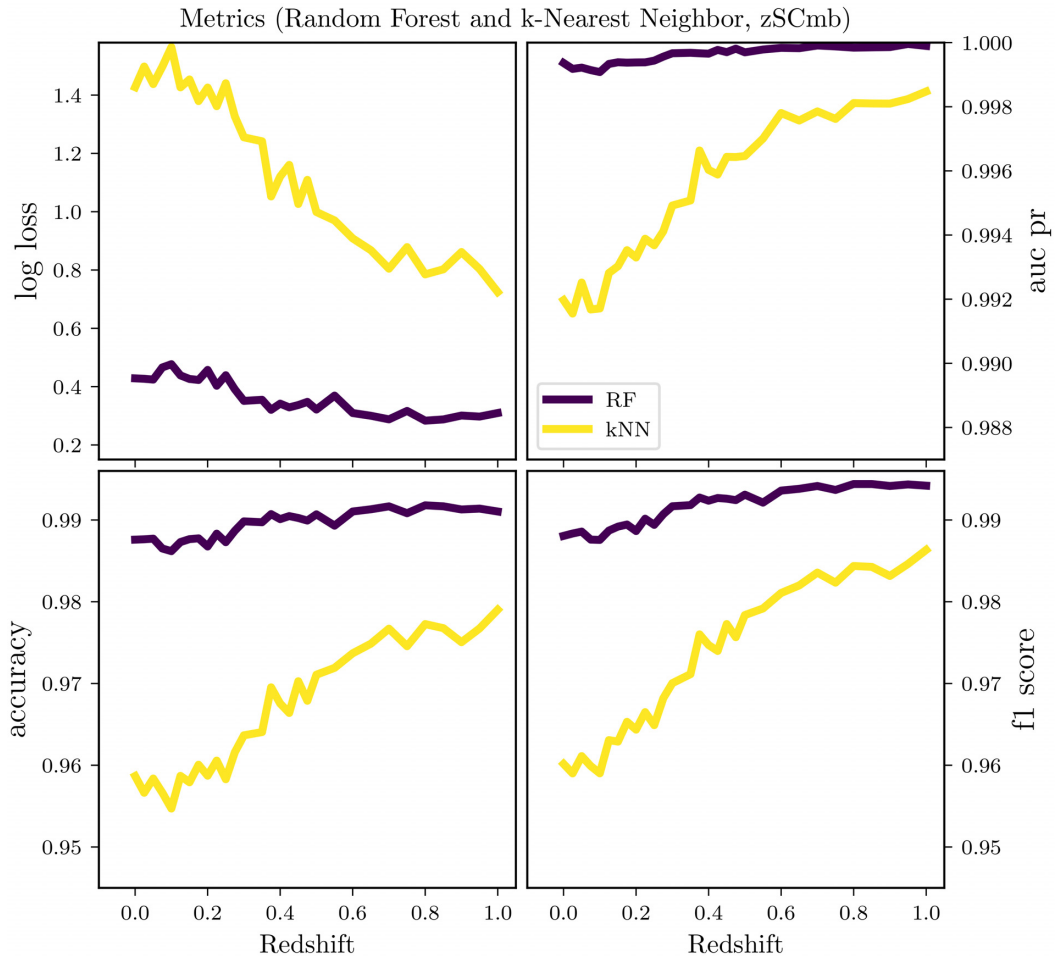


**Figure 3.** Four metrics as a function of  $z$  of both RF and kNN methods for zSCmb setup. Top left:  $\log$  loss, top right:  $AUC PR$ , bottom left:  $accuracy$ , and bottom right:  $f_1$ .

nearest neighbour) shows values  $\sim 0.95$ , while DNN’s performance is consistently poorer.

The dependencies of both  $accuracy$  and  $f_1$  on redshift follow similar trend; they both increase as we go to higher  $z$ . This anticorrelates with the regressor built in RAD18 since the latter has a decreasing performance at higher  $z$ . This looks somehow promising since the incline and decline of the classifier and regressor with increasing  $z$  respectively add up to an even performance of their combination up to  $z = 1$ . At  $z > 1$ , the performance of the classifier also degrades. That limitation is the reason we only show the results up to  $z \sim 1$ . In other words, most of the H I-poor galaxies can be filtered out by the classifier such that the regressor will only estimate the gas content of the H I-rich galaxies.

As expected, the value of the  $accuracy$  and that of  $f_1$  when training the learners with all the data available between  $z = 0-0.5$  is approximately the average of  $accuracy$ ’s and that of  $f_1$ ’s within that  $z$ -bin. As already mentioned in RAD18 the main idea behind the ‘ $f$ -training’ is to anticipate the fact that in real observations, retrieving redshift information is not an easy task. Therefore we make an attempt at also building a classifier without relying on redshift information. The high values of both  $accuracy$  and  $f_1 \sim 0.9$  for all learners with any setup except fSMg demonstrate that it is indeed possible to build a relatively good classifier without taking into account redshift information.

#### 4.2 Dependence on input features

We now look in more detail at how the classification is affected by the selected input features, i.e. comparing the rows in Fig. 2. In realistic scenarios, it is not always possible to have all the features available. This leads us to investigate different scenarios by considering different combinations of features. The best classifier (RF) does appear to be insensitive to the choice of input features with values of  $accuracy$  and  $f_1 \geq 0.98$  at all redshift bins, which is good news. However, for the learner with the worst performance (GRAD), it does not seem to be the case as its performance measures fluctuate with respect to the setup considered and are at their lowest values with zSMg setup (at  $z = 0$ ,  $f_1$  and  $accuracy$  are both  $\sim 0.87$ ;  $z = 1$ ,  $f_1 \sim 0.91$ , and  $accuracy \sim 0.88$ ) for ‘ $z$ -training’ and  $accuracy \sim 0.857$  and  $f_1 \sim 0.877$  for ‘ $f$ -training’ fSMg.

In Fig. 3, we show other metrics of the RF, namely  $AUC PR$  and  $\log$  loss, as function of redshift for zSCmb. As expected, the better performance at higher redshift bin corresponds to a lower  $\log$  loss. An  $AUC PR \geq 0.99$  at all redshifts corroborates the fact that RF is our best classifier for this ideal scenario where classifiers are both trained and tested with mock data.

It is noted that the effects of the class imbalance – potential issue owing to a big difference between the number of instances of each class in the training set which might cause a classifier to fail to label new instances in the test set properly – has been accounted for by

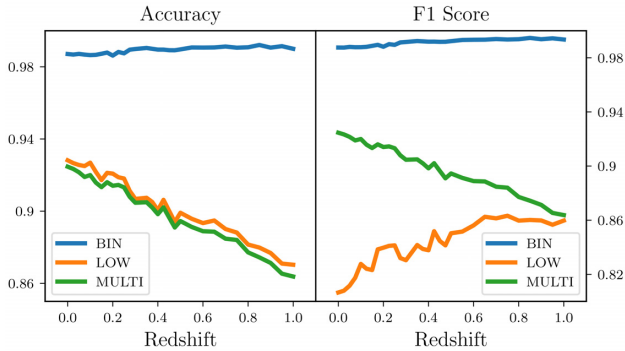


**Figure 4.** Left-hand panel: *accuracy* as function of  $z$ , and right-hand panel:  $f_1$  as a function of  $z$ . Blue is for BIN, orange for LOW, and green for MULTI. The results are all related to RF algorithm.

using IMBLEARN (Chawla et al. 2002) which is an oversampling method. No noticeable difference has been found between the two cases – with and without compensation – by comparing their resulting metrics.

### 4.3 Effects of setting up the classes

In our main analyses, the H I galaxies are split into two distinct classes according to whether their H I gas masses are above or below a threshold of 0.01 times their stellar masses. The threshold value is broadly in accordance with observational H I fraction limits. However, other classifications are possible. Here, we explore the impact of changing the classification metric.

We consider three new classification schemes.

(i) The Galex Arecibo SDSS Survey (GASS; Catinella et al. 2013) set a threshold limit of  $\log(M_{\text{HI}}) = 8.7$  for galaxies with  $M_* < 10^{10.5} M_\odot$  and  $\log(M_{\text{HI}}/M_*) = -1.8$  otherwise. However, in order to be consistent with the threshold value of gas fraction used in RAD18 to denote H I-depleted galaxies, we set it to be  $\log(M_{\text{HI}}/M_*) = -2$ . We call this type of splitting BIN.

(ii) Another potential classification may be on whether a galaxy has higher H I mass than stellar mass. In this case, the classes are given by  $\{\log(M_{\text{HI}}/M_*) < 0 \rightarrow 0; \log(M_{\text{HI}}/M_*) \geq 0 \rightarrow 1\}$ . We name this type of splitting LOW.

(iii) Finally, we attempt splitting into *three* classes, as follows:  $\{\log(M_{\text{HI}}/M_*) < -2 \rightarrow 0; -2 \leq \log(M_{\text{HI}}/M_*) < 0 \rightarrow 1; \log(M_{\text{HI}}/M_*) \geq 0 \rightarrow 2\}$ , which we call MULTI.

In Fig. 4, we compare the results corresponding to the RF method when considering three types of splitting, namely BIN (blue), LOW (orange), and MULTI (green). For brevity we only consider RF, since it is our best classifier, and  $z$ -training since the  $f$ -training values are expected to be similar.

Overall, both *accuracy* and  $f_1$  are  $\geq 0.80$  for all three types of splitting at all  $z$  bins and it is quite clear that the algorithm performs best with our main type of splitting H I poor/H I rich, namely BIN. It is also interesting to see that the *accuracy* decreases with increasing redshift for both LOW and MULTI, whereas  $f_1$  increases as we go at higher redshift for LOW. Based on *accuracy*, the method performs similarly for LOW and MULTI splittings, but the difference in performance of the algorithm is striking when considering  $f_1$  as a metric. This indicates that the classifier performance does depend on the classes chosen, but for our purposes of separating H I-rich and

H I-poor galaxies, it performs very well even with minor changes to the scheme.<sup>5</sup>

It is worth noting that in this idealized case and in the light of the results in RAD18 we did not include SVM (support vector machine) method. However, as will be shown later, we include it for the different tests on real observation data.

## 5 APPLICATION TO OBSERVATIONAL DATA

The lack of available data is one of the drawbacks of using machine learning when solving a problem, be it regression or classification. To mitigate that issue, in the context of H I study, we aim at building classifiers trained with mock data from simulation and using them to identify H I-rich galaxies in real surveys.

As already demonstrated in RAD18 the regressors that they built were able to learn from the mock data in order to predict the H I content of the galaxies from both RESOLVE and ALFALFA. Our approach here is to redo the same exercise but for a classification task, i.e. training some classifiers with MUFASA data and utilizing them to identify H I rich galaxies from the same surveys, RESOLVE and ALFALFA. In this study, we also consider another survey, GASS, in which both H I-poor and H I-rich galaxies are better represented for our tests. For the description of the first two surveys, we refer the interested reader to RAD18, and will now give a brief description of GASS.

### 5.1 GALEX Arecibo SDSS Survey data

GASS was aimed at investigating H I properties of a selected sample of galaxies ( $\sim 1000$ ) with available optical properties. The last data release (DR3, Catinella et al. 2013), which we use in our analyses, was built upon the first two DRs (Catinella et al. 2010, 2012). Within a relatively large volume survey of 200 Mpc already probed by SDSS primary spectroscopy survey, the GALEX Medium Imaging Survey and ALFALFA, galaxies have stellar masses of  $10 < \log(M_*/M_\odot) < 11.5$  that encompasses the transition mass. The targets have H I richness above the detection limit of 0.015 for  $10.5 < \log(M_*/M_\odot)$  and a fix H I mass of  $10^{8.7} M_\odot$  for lower stellar masses. The targets are designed to fall within  $0.025 < z < 0.05$ .

Using the Arecibo radio telescope, Catinella et al. (2013) compiled a sample which has a fairly good representation<sup>6</sup> in which 62 per cent are referred to as *detections* and the remaining 38 per cent as *non-detections*. The latter represent galaxies in which a relatively small gas mass fraction was observed hence required a longer integration time (but not more than 3 h), whereas the former was found to have relatively large amount of gas mass fraction. For our analyses, we retrieved all the optical properties of each galaxy in the sample from SDSS data base using their SDSS-ID. In order to have a more balanced test sample, we then split the sample into two classes: H I-poor galaxies (class 0) are those with  $\log(M_{\text{HI}}/M_*) < -1.55$  and the remaining are H I-rich galaxies (class 1). With this type of splitting, we have 56.8 per cent of the sample H I rich and the remaining H I poor. Our choice of adopting a higher H I detection limit is solely based on our aim to have a more balanced classes in both training and testing sets, and not on any scientific ground. Catinella et al. (2013) chose to use a threshold of about  $-1.8$  which is lower than what we use here. For the upcoming LADUMA survey, this value could be the same or different.

<sup>5</sup>Slight change to the gas fraction limit.

<sup>6</sup>GASS *representative* sample as they call it.

**Table 2.** Summary of the results when using the simulation trained methods to classify H I galaxies in the three different test tests.

	Accuracy	$f_1$	ROC AUC	Precision	Specificity
<b>TEST 1</b>					
RF	0.974	0.987	0.633	0.979	0.0
GRAD	0.962	0.980	0.788	0.979	0.0
$k$ NN	0.897	0.945	0.742	0.987	0.428
DNN	0.979	0.989	0.589	0.980	0.0
SVM	0.734	0.844	0.721	0.991	0.714
<b>TEST 2</b>					
RF	0.774	0.870	0.829	0.991	0.666
GRAD	0.597	0.741	0.822	0.998	0.952
$k$ NN	0.710	0.827	0.738	0.990	0.666
DNN	0.834	0.909	0.747	0.983	0.286
SVM	0.742	0.849	0.781	0.993	0.761
<b>TEST 3</b>					
RF	0.948	0.973	0.953	1.0	1.0
GRAD	0.881	0.937	0.970	1.0	1.0
$k$ NN	0.882	0.937	0.900	1.0	1.0
DNN	0.854	0.921	0.435	1.0	0.0
SVM	0.848	0.917	0.893	1.0	1.0
<b>TEST 4</b>					
RF	0.642	0.659	0.685	0.717	0.683
GRAD	0.624	0.631	0.682	0.713	0.700
$k$ NN	0.550	0.348	0.618	0.985	0.995
DNN	0.732	0.761	0.666	0.767	0.418
SVM	0.717	0.702	0.809	0.876	0.891

## 5.2 Testing the built classifiers

We consider four different tests according to both the survey and input features

(i) **TEST 1:** RESOLVE DATA, colour indices from all the band magnitudes available; SDSS ( $u, g, r, i, z$ ), Two Micron All-Sky Survey or 2MASS ( $J, H, K$ ), Galaxy Evolution Explorer or GALEX ( $NUV$ ), and UKIRT Infrared Deep Sky Survey or UKIDSS ( $Y, H, K$ ).

(ii) **TEST 2:** RESOLVE DATA, colour indices from only SDSS ( $u, g, r, i, z$ ) photometric data.

(iii) **TEST 3:** ALFALFA, colour indices from only SDSS ( $u, g, r, i, z$ ) photometric data.

(iv) **TEST 4:** GASS data, colour indices from only SDSS ( $u, g, r, i, z$ ) photometric data.

In all cases we split the simulated data for training and the considered test set into two categories, H I poor (class 0) and H I rich (class 1). Our results are summarized in Table 2 and shown in Fig. 5.

## 5.3 TEST 1

The training set is composed of the data of snapshot at  $z = 0$  from MUFASA, since the galaxies to be classified in RESOLVE survey are all at present epoch. We make use of all the photometric data available in RESOLVE, i.e.  $\{u, g, r, i, z, J, H, K_s, NUV\}$ . We consider five metrics – accuracy,  $f_1$ , ROC AUC, precision, and specificity. The results of the classification from the learners selected in this work are presented in Table 2 and similarly shown in Fig. 5.

DNN has the highest accuracy amongst the algorithms followed by RF. This is reminiscent to the results found in the regression problem in RAD18. Despite the weaker performance of DNN compared to RF when testing on the simulated data (see Fig. 2),

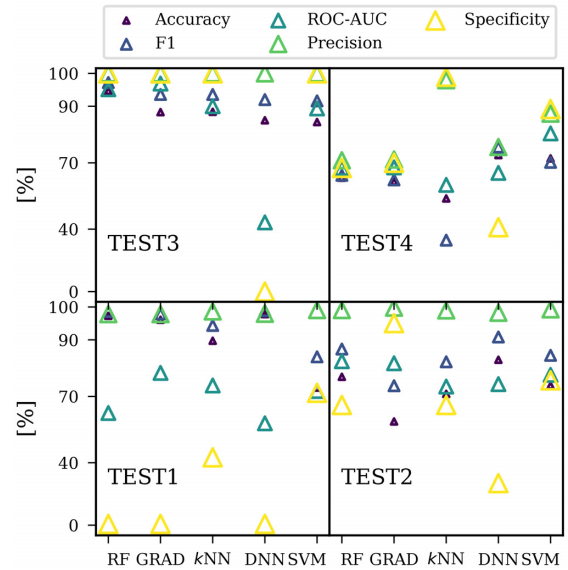


**Figure 5.** Summary of the results when using the simulation trained methods to classify the H I content of galaxies from three different test sets from observational data. The y-axes are in exponential scale to prevent for data point cluttering.

testing on observational data really show the power of the algorithm. Nonetheless, all algorithms agree within  $< 10$  per cent. Based on the  $f_1$  score and precision the methods are all comparable as well. Interestingly, DNN’s ROC AUC = 0.589 is the worst among all the methods, just above that of a classifier with a random guess.

Judging by the values of the precision which are  $\geq 0.95$  for all methods, they satisfy what we require; classifiers that minimize the number of H I-poor galaxies incorrectly classified as H I rich ( $FP$ ) or in other words with high precision. However, a specificity equal to zero implies that all the negative class instances in the data are incorrectly classified ( $FP$ ), bearing in mind that only 2 per cent of this test sample are H I-poor galaxies. Along with its high precision, SVM exhibits the highest specificity = 0.714, indicating its robustness, hence the best choice among the algorithms for this test.

We finally note that although  $\sim 98$  per cent for the RESOLVE galaxies are H I-rich, MUFASA sample contains a balanced proportion of  $\sim 52$  per cent positive class making the training robust against class imbalance effect. The most important thing is the training part which is achieved using a well-balanced sample (50/50 poor-rich), therefore the algorithms are not biased toward any class. In Test 4, we will consider a testing set that is more balanced (albeit smaller), which allows us to test our algorithm more fully.

## 5.4 TEST 2

For this second test, we still use the RESOLVE data but consider colour indices formed out of SDSS photometric data only, i.e.  $\{u, g, r, i, z\}$ . In contrast with TEST 1, the results in Table 2 (Fig. 5) suggest that, with the selected inputs features, the methods are capable of better identifying the gas-poor galaxies with specificity all above 0.5, except for DNN with 0.286. In terms of Accuracy and  $f_1$  scores, DNN is remarkably better and GRAD noticeably worse compared to RF and  $k$ NN. Based on ROC AUC, RF, and  $k$ NN score the best and worst, respectively. Based on the value of its precision = 0.998, it is tempting to say

that GRAD is the best method for this test, however the results suggest that SVM generalizes better than GRAD, as indicated by its  $f_1$  score and *accuracy*. It is quite surprising to notice that with the same data (training/test), decreasing the number of selected features provide better information to the algorithms such that they get better at classifying the instances properly *i.e.* *precision* (TEST 2) > *precision* (TEST 1); *specificity* (TEST 2) > *specificity* (TEST 1).

### 5.5 TEST 3

In this test, we use ALFALFA data and only consider SDSS photometric data for the input features as in TEST 2. Overall, all the methods perform much better as suggested by the high values of the metrics considered (see Table 2). We note that the training set is the same as the one used for RESOLVE, hence class imbalance is not an issue that requires to be alleviated during training. The *precision* and *specificity* which are both equal to 1 clearly imply that *FP* is zero, hence class 0 instances, despite their relatively low number, are all correctly classified. This applies to all classifiers with the exception of DNN which has a *specificity* = 0. The results for this test then suggest that our classifiers are capable of recognizing HI-rich and HI-poor galaxies to a very good precision. The  $f_1$  scores (all >0.9) of all the learners show that their *recall*'s are optimized, which also means that *FN* (HI-rich galaxies that incorrectly classified as HI poor) is minimized. The relatively higher average precision (*ROC AUC*) of all classifiers (> 0.9) can indeed be used as an indicator that on average both *FP* and *FN* are minimized, this is not the case for DNN. All the trained non-neural network algorithms appear to meet our requirements but for the sake of comparison, RF method seems to be the best in this test, with the highest *accuracy* and  $f_1$  values despite its *ROC AUC* is only second best. Conversely with the RESOLVE data, the DNN is definitely not favoured in properly classifying HI-poor and HI-rich galaxies when tests are done with blind survey data such as ALFALFA.

### 5.6 TEST 4

We use GASS data (Catinella et al. 2013) for this test, considering SDSS photometric data as input features. Unlike the other samples used for testing so far, all classes (0, 1) are well represented in this data set, with 56 per cent of this test set are HI rich. Although *k*NN exhibits the highest precision and specificity, it does not generalize well, given its relatively low values of both *accuracy* and  $f_1$ . Results suggest that our best classifier for this test is SVM which has a relatively high precision (second best after *k*NN) and its tendency to generalize well as justified by its overall scores. The confusion matrix shown in Fig. 6 and the precision-recall curve for SVM (blue line) in Fig. 7 come to corroborate the fact that SVM method is capable of generalizing well. A classifier with random guess is shown with the diagonal dashed line for reference. The further from the diagonal the classifier is, the better its quality. The average precision is 0.858 (represented by the red dashed line). It is obtained by averaging the different precision values from the different thresholds. In general, the other classifiers (RF, GRAD, and DNN) are also capable of learning the features from the mock data in order to classify the real data, except the neural network model which poorly classifies the HI-poor galaxies (*i.e.* low *specificity* values), as can be noticed in all the tests conducted. To further illustrate, we show in Fig. 8 the distributions of probabilities of GASS instances to be gas rich (blue line) or gas poor (orange line) as predicted from the SVM-trained model. Both distributions

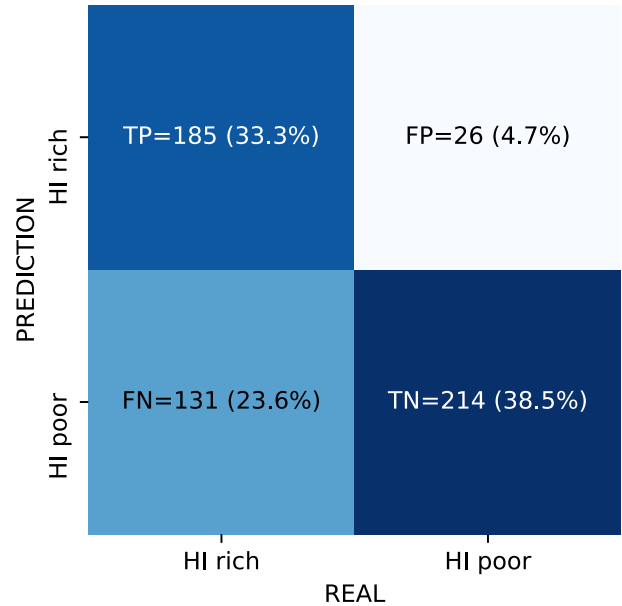


**Figure 6** 2 x 2 confusion matrix for a binary classification from SVM in TEST 4. Positive class is HI rich and Negative class is HI poor.

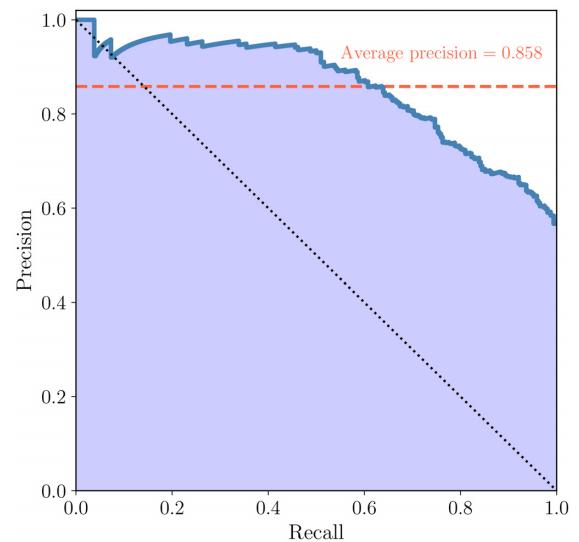


**Figure 7.** Precision-recall curve obtained from SVM in Test 4. The dashed red line denotes the average precision (0.858), whereas the dotted line indicates performance of a classifier with random guess.

are dominated by high values ( $\sim 1$ ), indicative of a better classifier, although we still notice considerable fractions of low probabilities. Provided that the two classes are well represented in GASS data set, which makes this latter a better test set compared to the others, we present the set of hyperparameters used for each algorithm in Table. 3. It is noted that for each of the non-neural network based methods, we only show the hyperparameters that are different from the default values given in SCIKIT-LEARN (Pedregosa et al. 2011).

## 6 DISCUSSION AND CONCLUSION

We have demonstrated in this work that it is possible to classify HI galaxies based on their gas content using both their photometric and environmental data. We have built various algorithms by

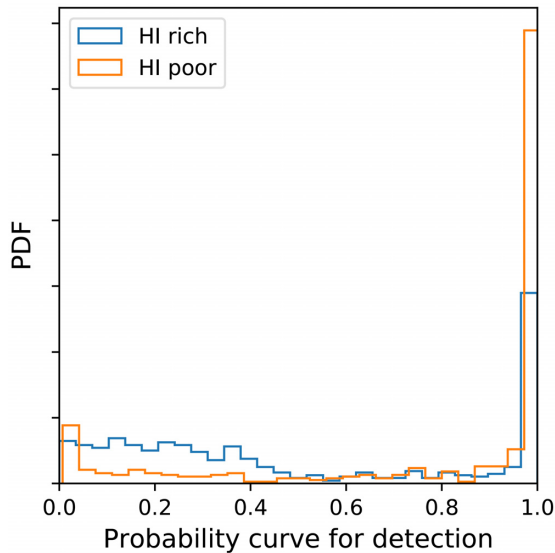


**Figure 8.** Distribution of probabilities for detecting H I-rich (blue) and H I-poor (orange) galaxies from the SVM classifier on the fSCmb setup of the GASS data.

**Table 3.** Summary of the hyperparameters used for each type of classifier in TEST 4.

Hyperparameters	
RF	Number of base estimators = 100
GRAD	Number of base estimators = 50
$k$ NN	Number of neighbours = 3
DNN	$3^\dagger$ , $100^\diamond$ , relu $\clubsuit$ , adam $\spadesuit$ , Yes $\ast$ , $32^\Delta$ , $5^\ddagger$
SVM	Kernel = radial basis function, $C = 100$ , $\gamma = 0.3$

Notes:  $\dagger$  Number of layers.

$\diamond$  Number of nodes per layer.

$\clubsuit$  Activation function.

$\spadesuit$  Optimizer.

$\ast$  Batch normalization.

$\Delta$  Batch size.

$\ddagger$  Number of epochs.

training them using large subset of the mock data (80 per cent) from MUFASA simulation. While being sensitive to:

- (i) the inputs features,
- (ii) type of training ( $f$ -training or  $z$ -training),
- (iii) type of class splitting.

the test results, using smaller subset of MUFASA mock data (different from the subset on which they have been trained), look very promising. For instance, both *Accuracy* and  $f_1$  score  $> 0.9$ .

We have shown the good performance of the built classifiers when being tested on real observation data – RESOLVE, ALFALFA, and GASS surveys – after training them on the mock data from MUFASA. Our findings can be summarized as follows:

(i) On using MUFASA to both train and test the learners, RF shows the best performance amongst the learners with an *Accuracy* of 99.00 per cent *ROC AUC* above 99.96 per cent,  $f_1$  score 99.4 per cent at  $z = 1$ . Other classifiers like  $k$ -NN and DNN also perform similarly well in general, however GRAD method shows poor performance when considering  $z$ SMg and fSMg setups.

(ii) For  $z$ -training, *Accuracy* and  $f_1$  score increase from present to higher redshift. The increase is steeper at  $z < 0.5$  and flattens out

at higher redshift. This indeed compensates the fact that regressors built in RAD18 perform best at low redshift and more poorly with increasing  $z$ .

(iii) The performances of the classifiers appear to be insensitive to the selected input features for the training except with the case of GRAD method which struggles to properly classify the galaxies in the test set when only considering SDSS magnitudes and environmental information as input features ( $z$ SMg and fSMg).

(iv) The results are affected by the definition of the class of galaxies (BIN, LOW, and MULTI). BIN, which is the type of splitting behind the motivation for this work, corresponds to better results compared to the other two types of splittings.

(v) Comparing the results corresponding to four different tests using real observational data from RESOLVE, ALFALFA, and GASS surveys, with the exception of DNN as suggested by its low value of *ROC AUC* and zero *specificity*, the classifiers perform best on TEST 3 in which the test set is ALFALFA data and the input features considered are colour indices formed out of SDSS magnitudes only. All learners correctly classified the H I-poor galaxies with a *specificity* = 1.0 and their precision is also maximized (*precision* = 1.0), which is what we really aim for. For TEST 3, it is quite clear that most of the errors (if not all) come from *FN*, i.e. H I-rich galaxies misclassified as H I-poor, although this quantity is already minimized given the rather high  $f_1$  score of all the learners. By comparing TEST 1 and 2, it is clear that using colour indices from SDSS data only is the optimal option to better identify the H I-poor galaxies given the higher *precision* in TEST 2. DNN has the highest *Accuracy* and  $f_1$  for TEST 1 and TEST 2, indicative of being robust in classifying the H I-rich galaxies. However, DNN fails to achieve a reasonable classification of the H I-poor galaxies as shown by the low values of *Specificity* ( $< 0.3$ ) for all tests. The relatively poor performance of DNN<sup>7</sup> quantified by the slightly lower values of *Accuracy* and  $f_1$  for TEST 3 compared to TEST 1 and TEST 2 might be due to the nature of the test samples. We speculate that the neural network is able to achieve higher performance in a cleaner set of data such as from the RESOLVE survey but underperform in a sample from blind survey data such as ALFALFA. This does not mean the learner itself is not performing well, it only means that the data to test on are prone to higher systematic errors.

(vi) In TEST 4, we use a test sample from GASS, which unlike the other samples used in the first three tests, has a fairly good representation of the two classes (i.e. H I rich–H I-poor). This makes it a good data set for assessing how well the classifiers are able to apply the learned features from the mock data. Based on the most important performance metric in this study,  $k$ -NN is the best classifier for TEST 4 with a *precision* = 0.985. It also classifies the H I-poor galaxies properly as demonstrated by its high *specificity* (0.995). However, even though our purpose is to build a classifier that has a very good *precision* which translates to its ability to correctly classify H I-rich galaxies, in all kinds of machine-learning tasks, the algorithm that can minimize the generalization errors well is the more preferable. In this case specifically, as the results suggest, SVM proves to be able to generalize well as shown by its average *precision* of 0.858, *accuracy* (0.717),  $f_1$  score (0.702), *ROC AUC* (0.809), and both *precision* and *specificity* are the second best.

(vii) Overall in terms of performance, based on the scores in all tests on real data, we find that SVM is the best classifier as it demonstrates quite well its generalization ability, learning from simulated data in order to classify real data.

<sup>7</sup>Compared to other classifiers in this test.

With the advent of large H I surveys like LADUMA and MIGH-TEE, we have presented the possibility of properly classifying galaxies according to their gas content, using machine learning. The robustness of our methods lie in the fact that the trained algorithms can learn from mock data in order to classify galaxies in real surveys, which is indeed a strong asset in the sense that in reality the lack of enough data to train the methods turns out to be an issue that requires to be mitigated. Together with the regressors built in RAD18, the classifiers in this work will form a useful pipeline to create mock H I surveys for assisting with survey design, and eventually, will enable more detailed tests of the input model by comparing observed H I to that predicted from the regressor on a case-by-case basis.

We only analysed the performance of single models in both this work and RAD18. However, the use of more complex models using ensemble or stacking techniques are increasingly favoured in the literatures. We will explore such methods in future work despite their level of complexity as well as their interpretability.

## ACKNOWLEDGEMENTS

SA acknowledges financial support from the *South African Radio Astronomy Observatory* (SARAO). MR and RD acknowledge support from the South African Research Chairs Initiative and the South African National Research Foundation. Support for MR was also provided by the SKA post-graduate bursary program. The MU-FASA simulations were run on the Pumbaa astrophysics computing cluster hosted at the University of the Western Cape, which was generously funded by UWC's Office of the Deputy Vice Chancellor. Additional computing resources are obtained from the Max Planck Computing and Data Facility (<http://www.mpcdf.mpg.de>) and South African Radio Astronomy Observatory (SARAO).

## REFERENCES

- Catinella B. et al., 2010, *MNRAS*, 403, 683  
 Catinella B. et al., 2012, *A&A*, 544, A65  
 Catinella B. et al., 2013, *MNRAS*, 436, 34
- Chawla N. V., Bowyer K. W., Hall L. O., Kegelmeyer W. P., 2002, *J. Artif. Intell. Res.*, 16, 321  
 Colless M., Morganti R., Couch W., 1998, in Morganti R., Couch W. J., eds, *ESO/Australia Workshop*. Springer, Berlin  
 Davis T. A. et al., 2011, *MNRAS*, 417, 882  
 Davé R., Rafieferantsoa M. H., Thompson R. J., Hopkins P. F., 2017, *MNRAS*, 467, 115  
 Donahue M., de Messières G. E., O'Connell R. W., Voit G. M., Höffer A., McNamara B. R., Nulsen P. E. J., 2011, *ApJ*, 732, 40  
 Fernández X. et al., 2016, *ApJ*, 824, L1  
 Folkes S. et al., 1999, *MNRAS*, 308, 459  
 Foltz R. et al., 2018, *ApJ*, 866, 136  
 Fossati M. et al., 2017, *ApJ*, 835, 153  
 Fukugita M. et al., 2007, *AJ*, 134, 579  
 Gauci A., Adami K. Z., Abela J., 2010, preprint ([arXiv:1005.0390](https://arxiv.org/abs/1005.0390))  
 Haynes M. P. et al., 2011, *AJ*, 142, 170  
 Haynes M. P. et al., 2018, *ApJ*, 861, 49  
 Hess K. M., Wilcots E. M., 2013, *AJ*, 146, 124  
 Huertas-Company M., Rouan D., Tasca L., Soucail G., Fevre O. L., 2008, *A&A*, 478, 971  
 Koekemoer A. M. et al., 2007, *ApJS*, 172, 196  
 Lahav O., Nairn A., Sodr e L., Storrie-Lombardi M., 1996, *MNRAS*, 283, 207  
 Morgan W. W., Mayall N., 1957, *PASP*, 69, 291  
 Naim A., Lahav O., Sodre L., Jr, Storrie-Lombardi M., 1995, *MNRAS*, 275, 567  
 Pedregosa F. et al., 2011, *J. Mach. Learn. Res.*, 12, 2825  
 Planck et al., 2016, *A&A*, 594, A13  
 Rafieferantsoa M., Andrianomena S., Dav e R., 2018, *MNRAS*, 479, 4509  
 Rafieferantsoa M., Dav e R., Angl es-Alc azar D., Katz N., Kollmeier J. A., Oppenheimer B. D., 2015, *MNRAS*, 453, 3980  
 Rafieferantsoa M., Dav e R., Naab T., 2019, *MNRAS*, 486, 5184  
 Slonim N., Somerville R., Tishby N., Lahav O., 2001, *MNRAS*, 323, 270  
 Stark D. V., 2016, *ApJ*, 832, 126  
 Teimoorinia H., Ellison S. L., Patton D. R., 2017, *MNRAS*, 464, 3796  
 York D. G. et al., 2000, *AJ*, 120, 1579  
 Zaritsky D., Zabludoff A. I., Willick J. A., 1995, *AJ*, 110, 1602

This paper has been typeset from a  $\text{\TeX}/\text{\LaTeX}$  file prepared by the author.